Desalination and Water Treatment
www.deswater.com

doi: 10.5004/dwt.2021.27784

242 (2021) 214–220
December

Selection and optimization of the control plan for precipitation characteristic landslide

Liangting Wang, Zhishan Zheng*, Xijian Chao, Huojun Zhu

Jiangxi University of Engineering, Xinyu, Jiangxi 338000, China, email: zhishanzheng5hz@yeah.net (Z. Zheng)

Received 20 August 2021; Accepted 23 September 2021

ABSTRACT

The purpose is to prevent the occurrence of precipitation characteristic landslide disasters. A precipitation characteristic landslide is selected as the research object, and the prevention and control of precipitation characteristic landslide disasters are studied. First, the stability of the precipitation characteristic landslide is analyzed, and the research methods are introduced, mainly including the transfer coefficient method and Finite Element Strength Reduction Method (FESRM). Second, based on the research methods, Midas Geotechnical and Tunnel Analysis System software is used to establish a two-dimensional model for controlling the precipitation characteristic landslide under natural conditions. Finally, an anti-sliding control plan is made: The slope in the front section of the landslide is lowered, and the anti-sliding device is installed in its rear section. The results show that the stability coefficient of the slope in the front obtained by the transfer coefficient method is 1.085 and that obtained by FESRM is 1.080. The difference ratio between the two values is 0.5%. After deceleration in the front part of the precipitation characteristic landslide is done, the stability coefficient is 1.021, which is 2.8% lower than before. When the horizontal component of residual thrust is taken as 1,360 kN/m after the anti-sliding is conducted, the active earth pressure is 887 kN/m, and the horizontal component of residual thrust is greater than that of active earth pressure. The thrust value of the anti-sliding device is designed as 1,360 kN/m, and the residual thrust curve in the designed conditions is above the curve in the check working condition, this proves that the designed condition is safe. The internal forces of the anti-sliding device are as follows: the maximum bending moment is 20,123.24 kN/m, the maximum shear force is 4,881.01 kN, the maximum lateral stress is −718.44 kPa, and the anchorage depth is 859 kPa > 718.44 kPa. This shows that the depth calculation is qualified. The stability coefficient of the cross-section after the control of the anti-sliding device is 1.15, which is improved to a certain extent, but it is less than the theoretical value of 1.20 and needs to be optimized. The control plan is optimized by adding an anchor cable to the anti-sliding device. The control plan designed in this study has a good effect on controlling landslides.

Keywords: Precipitation characteristic landslide control; Transfer coefficient method; Strength reduction method; Scheme optimization

1. Introduction

China has a vast territory, and nearly three-quarters of the land is mountainous [1]. Mountainous areas are prone to geological disasters due to their unique landforms. Common geological disasters include collapse, precipitation characteristic landslide, and debris flow, which are mostly caused by precipitation [2]. A precipitation characteristic landslide refers to the geological phenomenon that the rock on the sloping land appears to stress maladjustment inside the slope under the action of gravity or external force, causing a downward slide [3]. The main causes of landslides are earthquakes, heavy rainfall, freeze-thaw, long-term creep, artificial disturbance, and so on. Among them, the landslide

* Corresponding author.

disasters caused by artificial disturbance are increasing year by year. With the wider geographic area of human activities and the increase of activities, the occurrence frequency of landslides increases accordingly. Among the geological disasters in 2020, landslides account for 69.28% [4]. As one of the most frequent geological disasters, landslides usually bring great hidden dangers to people's life and property [5]. How to prevent the occurrence of landslides is a major problem faced by human society [6], and landslide control research has important practical significance.

The research on precipitation characteristic landslide control in China experiences the stage of exploring the causes of precipitation characteristic landslides [7], studying the mechanism of landslide movement, and active prevention of landslides [8]. Nowadays, the mainstream research is on the relationship between landslides and climate in combination with modern advanced science and technology to achieve reasonable precautions, but the precautions and control methods still need to be improved [9]. At present, the theoretical research on landslide control is divided into two directions: qualitative research and quantitative research [10]. The quantitative research method is mainly the limit equilibrium method and numerical analysis method [11]. And the specific measures include the drainage of slope zones [12], the avoidance of steep slopes, and the reform of the slope [13]. In this study, the slope is segmented and then controlled to prevent the occurrence of landslides.

Based on stability analysis, the stability coefficients under the transfer coefficient method and the strength reduction method are compared, and the prevention and control plan of precipitation characteristic landslides is made. The landslide is segmented and then controlled, and the results of the prevention and control plan are analyzed. On this basis, an optimization design is proposed. The study has a reference for the research on landslide prevention and control in the future.

2. Design of the prevention and control plan of precipitation characteristic landslides

2.1. Overview of the study area

The landslide selected in this study has a subtropical monsoon climate, with four distinctive seasons, high temperature, much rain in summer, and mild climate, and little rain in winter. The annual average temperature is 14.8°C, and the annual minimum temperature appears in December, with an average of 4.9°C. The recorded minimum temperature is –8.4°C, and the highest temperature appears in July, with an average of 34.9°C. The highest temperature reaches 37.9°C. The most precipitation appears in summer, accounting for 80%~85% of the annual precipitation, and the average precipitation is 500~9,109 mm. There is southeast wind in summer and northwest wind in winter, and the maximum wind speed is 23.7 m/s. The groundwater in this landslide area is detected to be freshwater [14] and will not cause corrosion to concrete. And the area doesn't lie on the seismic belt and the crustal activities are few, so seismic activities are ignored in this study.

The landslide is located near the highway, belonging to the hilly landform with a slope gradient of 18°–29°. According to the landform, it belongs to the erosion landform. The vegetation in the study area is mainly weeds and pines. The landslide is mainly subjected to north-south fracture tension, and the fracture direction is inconsistent with the direction of the slope. There is a sign of loosening around the slope, and the slope is unstable. The stratum distribution in the slope is relatively simple, as shown in Fig. 1.

Fig. 1 shows that the stratum of the slope includes a quaternary residual layer and a clay layer. The landslide is caused by the destruction of regional balance after crops are changed. The average altitude of the whole landslide is 142 m. The landslide is located near the line between the ridge and valley, and the slopes on both sides of the landslide are 15°–33°. The whole slope shows a sign of forward sliding. There is no groundwater seepage near the slope. Based on the above, the region has the characteristics of a medium-sized shallow landslide.

The rock and soil composition in this region is mainly limestone, saprolite, and clay. The natural weight, direct shear force, and residual shear strength of the physical properties of clay in the geotechnical literature involved in this study are 16.9 kN/m^3, 34.5 kPa, and 31.9 kPa, respectively. And the natural weight, direct shear force, and residual shear strength of limestone are 18.2 kN/m^3, 32.8 kPa, and 28.8 kPa respectively, and its saturated compressive strength is 50 MPa. Since they directly affect the stability of the slope, the rock and soil mechanical parameters are estimated combined with the actual situation. The results show that the bulk density of the limestone is 20 kN/m^3, and its shear strength is 12.5 kPa; the bulk density of saprolite is 19 kN/m^3, and its bearing capacity and shear strength are 240 and 12 kPa respectively. The uniaxial compressive strength of the sliding bed is 32 MPa, the bulk density is 25 kN/m^3 and the bearing capacity is 1,400 kPa.

2.2. Stability analysis and the design of the prevention and control plan of the precipitation characteristic landslide in the study area

2.2.1. Stability analysis

Through field investigation, the cracks in the slope are new and old. Due to weathering, the rock and soil inside the

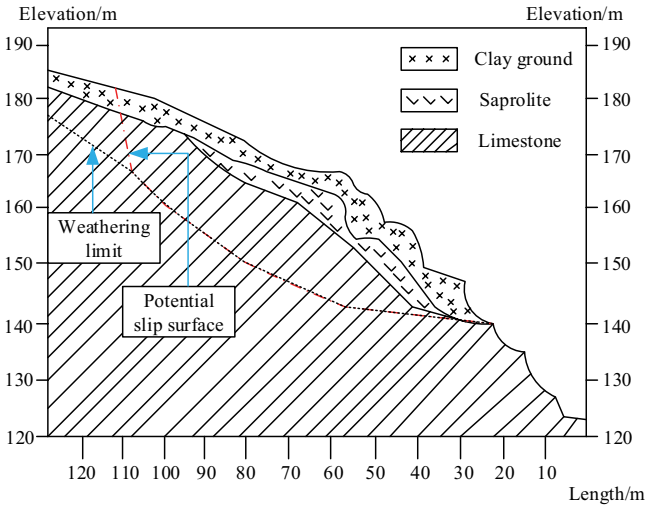

Fig. 1. Stratum distribution in the scope in the study area.

slope are relatively broken, the slope structure is not compact, and its mechanical properties are poor. If it rains, the slope will be continuously infiltrated by rain, leading to rock and soil sliding down and eventually causing landslides.

The transfer coefficient method is used to calculate the stability of the slope. The slope is assumed to be a piecewise ideal slip surface, and the overall sliding surface is composed of line segments. The reaction between segments is parallel to the overall sliding surface. The expression is shown in Eq. (1).

$$F_i = F_{st} \times T_i - R_i + P_{i-1}\Psi_{i-1} \tag{1}$$

where F_i is the sliding force of the slope in section i, F_{st} is the anti-sliding safety factor, T_i is the sliding force, R_i is the resistance force to the sliding, and Ψ_{i-1} is the transfer coefficient. The specific expressions are shown in Eqs. (2)–(4).

$$T_i = W_i \sin\alpha_i + Q_i \cos\alpha_i + T_{Di} \tag{2}$$

$$R_i = \left\{W_i\left[\left(1-r_u\right)\cos\alpha_i - \sin\alpha_i\right] - R_{Di}\right\}\tan\phi_i + C_i L_i \tag{3}$$

$$\psi_i = \cos\left(\alpha_{i-1} - \alpha_i\right) - \sin\left(\alpha_{i-1} - \alpha_i\right)\tan\phi_i \tag{4}$$

W_i in Eqs. (2)–(4) is the weight of section i, and in $W_i = \gamma \times s$, γ is the natural weight of the slope. S is the sliding area of section i. r_u is the void ratio, and its equation is $r_u = \frac{V_1 \times B_1}{V_2 \times B_2} = \frac{S_1}{2 \times S_2}$. In the equation, V_1 is the volume of the sliding body in water, V_2 is the total volume of the sliding body, B_1 and B_2 are the bulk density of water and sliding body, and S_1 and S_2 are the area in water and total area of the sliding body, respectively. R_{Di} is the seepage pressure on the vertical sliding surface, and its equation is $R_{Di} = \gamma_w h_{iw} L_i \tan\beta_i \sin(\alpha_i - \beta_i)$. T_{Di} is the seepage pressure on the parallel sliding surface, and its equation is $T_{Di} = \gamma_w h_{iw} L_i \tan\beta_i \sin(\alpha_i - \beta_i)$. C_i is the cohesion of the slope of section i. ϕ_i is the internal friction angle of the slope of section i. L_i is the length of the sliding surface of section i. α_i and β_i are the dip angle of the sliding surface in the ith section and the angle between groundwater flow direction and horizontal direction, respectively. γ_w is the weight of water.

The above equations are complicated. In this study, they are simplified by the transfer coefficient method [15], which reduces the calculation amount and meets the requirements for accuracy. The simplified equations are shown in Eqs. (5)–(8).

$$F_S = \frac{\sum R_i \Psi_i \Psi_{i+1} \ldots \Psi_{n-1} + R_n}{\sum T_i \Psi_i \Psi_{i+1} \ldots \Psi_{n-1} + T_n}, \left(i = 1,2,3,\ldots,n-1\right) \tag{5}$$

$$\Psi_i = \cos\left(\theta_i - \theta_{i+1}\right) - \sin\left(\theta_i - \theta_{i+1}\right)\tan\varphi_{i+1} \tag{6}$$

$$R_i = W_i \cos\theta_i \tan\phi_i + c_i l_i \tag{7}$$

$$T_i = W_i \sin\theta_i \tag{8}$$

In Eqs. (5)–(8), Ψ_i is the transfer coefficient of the calculation section i+1 in the parallel direction of the residual sliding force of section i, and θ_i is the dip angle of the sliding slope in section i.

In this study, the stability of the slope under natural (without rain) conditions is studied. The specific engineering parameters in the study area are applied to the above transfer coefficient equation, and they are shown in Eqs. (9)–(11).

$$F_S = \frac{T_{ki}}{T_{Hi}} \tag{9}$$

$$T_{ki} = \begin{bmatrix}\left(w_i - f_i\right)\cos\theta_i + D_i \sin\left(\theta_i - d_{wi}\right) \\ -E_{i-1}\sin\left(\theta_{i-1} - \theta_i\right)\end{bmatrix}\tan\phi_i + c_i l_i \tag{10}$$

$$T_{Hi} = \left[\left(w_i - f_i\right)\sin\theta_i - \cos\theta_i + E_{i-1}\cos\left(\theta_{i-1} - \theta_i\right)\right] \tag{11}$$

where T_{ki} is the resistance force of sliding, T_{Hi} is the sliding force, k is the anti-sliding stability coefficient of section i, w_i is the gravity of section i, θ_i is the angle between the sliding surface of section i and the horizontal plane, ϕ_i is the internal friction angle of the slider of section i, c_i is the cohesion at the sliding surface of the slope of section i, and f_i is the slope length of section i. D_i is the sliding force produced by the slope of section i under water pressure, and its equation is $D_i = \gamma_w x_{wi} i$. s_i is the buoyancy of section i in groundwater. E_{i-1} is the residual sliding force of the sliding block on segment i. The place at 65 m in the middle of the slope is dug up, and the data is input to calculate the stability of the profile [16].

Finite Element Strength Reduction Method (FESRM) is used to check the stability of the landslide. The principle of FESRM is shown in Fig. 2.

Fig. 2 shows that FESRM is used to calculate the stress cycle of the slope by using the finite element. After the optimization is conducted, the stress conditions of the section with a sign of sliding are obtained. Finally, the section of the slope that is most likely to slide is obtained based on the comparison [17].

The calculation based on FESRM can be found in Eqs. (12)–(15).

$$c' = \frac{c}{F_s} \tag{12}$$

$$\phi' = \arctan\left(\frac{\tan\phi}{F_s}\right) \tag{13}$$

$$\tau_f = c + \sigma\tan\phi \tag{14}$$

$$\tau = c' + \sigma'\tan\phi \tag{15}$$

where c is a cohesive force, ϕ is the internal friction angle, F_s is the reduction coefficient, c' is the reduced coefficient,

and ϕ′ is the reduced internal friction angle. According to the two definitions in the literature, the safety factor can be expressed as:

$$F_s = \frac{\tau_f}{\tau} = \frac{c + \sigma \tan\phi}{\tau} \tag{16}$$

$$F_s = \frac{c}{c'} = \frac{\tan\phi}{\tan\phi'} \tag{17}$$

Combined with the Eqs. (12)–(16) can be further expressed as:

$$F_s = \frac{c + \sigma \tan\phi}{c' + \sigma' \tan\phi'} \tag{18}$$

In this study, Midas GTS software is used for modeling on the basis of the strength reduction method. A two-dimensional model is used to simplify the calculation. Based on the previous literature, the parameters of the model are as follows: the grid width at the sliding slope is 2.2 m, the width of the lower boundary of the slope is 3.5 m, the partial grid value on the sliding surface is between 3 and 5 m, and the grid width around the sliding slope is 2.2 m. The left and right boundary of the slope is fixed horizontally, and the bottom of the slope is fixed in *X*-direction and *Y*-direction.

Because they influence the accuracy of FESRM, the geotechnical mechanical parameters are accurately selected combined with the actual situation of the study area based on the above data. The results are: the bulk density of the clay is 17 kN/m^3, the elastic modulus is 49 MPa, the Poisson's ratio is 0.25, the cohesion is 40 kPa, and the internal friction angle is 15°. The bulk density of limestone is 21, the elastic modulus is 2,000 MPa, Poisson's ratio is 0.38, cohesion is 50 kPa and internal friction angle is 25°. In this study, the elastoplastic model and Mohr-Coulomb criterion are selected based on the general situation of the research area [18].

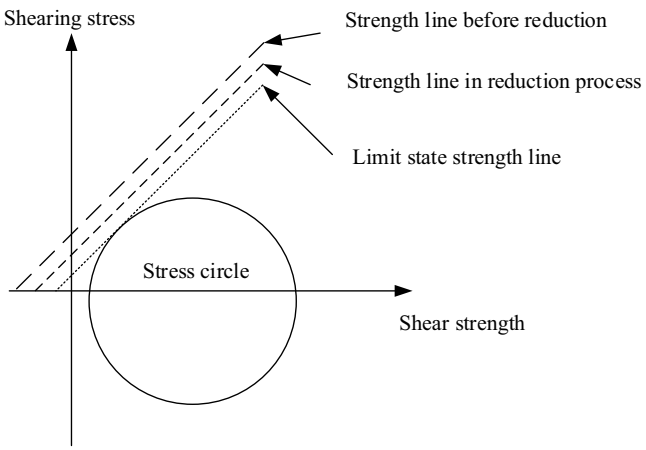

Fig. 2. Strength reduction.

2.2.2. Plan selection and design

The current landslide control plans mainly change the geotechnical structure of the landslide zone and the discharge form of groundwater, and increase the artificial support and the vegetation coverage of the landslide zone. If it encounters rainfall, the landslide will be aggravated. In this study, the plan is made for the landslide with increased rainfall, and the safety factor of the landslide is 1.1. Due to the loose rock and soil at the leading edge of the landslide and the sliding, the rear of the slope will have a landslide if it has no sufficient support force. Therefore, the slope is segmented and then controlled.

Due to the loose rock and soil in the front part of the slope, cracks appear. Once it rains heavily, it is very likely to cause rock and soil collapse. Therefore, on the basis of previous studies, the loose rock and soil are used in the front to lower the slope and reduce the downward speed. The lowered position is K_0 + 050 ~ K_0 + 150 outside the tunnel entrance of the study area, and the lowering rate is 1:1.6. The lowered section is shown in Fig. 3.

Fig. 3 shows that 5 m is reserved for construction in the front of the slope.

Based on previous studies, the anti-skid control of the rear section of the slope is carried out by using anti-skid devices. The anti-skid device is inserted into the stable rock and soil under the landslide surface to anchor with the stable rock and soil to prevent landslides. After the anti-sliding device is inserted into the slope, the section will be subjected to many forces, including the landslide thrust behind the device, the resistance of stabilizing rock and soil, and the resistance of the front of the device. The anti-sliding device is arranged in the front section of the landslide, and the device axis is located at 9 m inside the borehole.

The number of anti-slide devices is 8 according to the force of the slope, and the anti-slide device needs a pile with a large load and long size according to the size of the slope. The specific parameters of the anti-sliding device are as follows: the foundation coefficient is 2.5 × 105 kPa/m; the length of the pile in the anchorage section and the loading section is 9 m; the section height is 3 m; the width is 2.5 m;

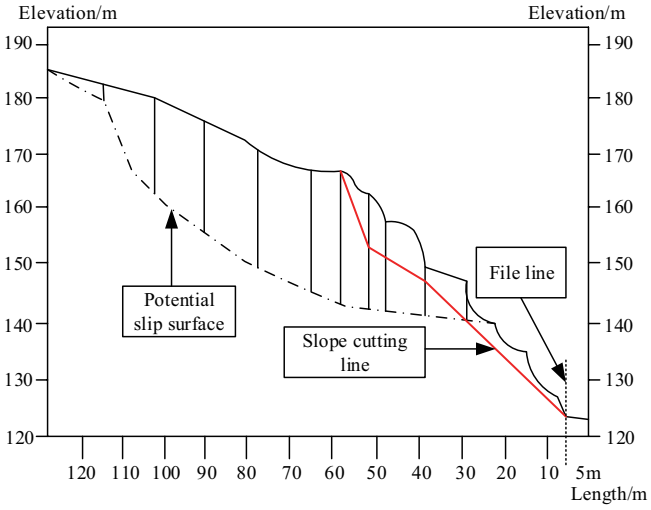

Fig. 3. Map of the lowered section.

the pile spacing is 3.5 m; the concrete grade of the device is C30; the elastic modulus of concrete is 3 × 104 MPa, and the bottom of the device is supported by the hinged end. In this study, the anti-sliding device is designed according to the elastic pile, and the thrust shape of the loading section of the slope is a triangle, which is analyzed based on the results of the field investigation.

The calculation method of the total internal force of the anti-sliding device is shown in Eq. (19):

$$\sigma_x = K \cdot B_p \cdot y_x \tag{19}$$

In Eq. (19), σ_x is the ground reaction, K is the foundation reaction coefficient (elastic resistance coefficient), B_p is the calculated size of the device, and y_x is its displacement.

The specific calculation equation of the internal force in the study area can be obtained from the analysis of specific parameters in this study, as shown in Eq. (20).

$$X_A = \frac{M_A}{\beta^2 EI}\frac{4\phi_3\phi_4 + \phi_1\phi_2}{4\phi_1\phi_3 - \phi_1\phi_4} + \frac{Q_A}{\beta^3 EI}\frac{4\phi_4^2 + \phi_2^2}{4\phi_2\phi_3 - \phi_1\phi_4} \tag{20}$$

$$Q_A = \frac{-M_A}{\beta EI}\frac{\phi_1^2 + 4\phi_2^2}{4\phi_2\phi_3 - 4\phi_1\phi_4} - \frac{Q_A}{\beta^2 EI}\frac{4\phi_3\phi_4 + \phi_1\phi_2}{4\phi_2\phi_3 - 4\phi_1\phi_4} \tag{21}$$

In Eqs. (20) and (21), E is the elastic modulus of the device, I is the inertia moment of the device section, and ϕ is the influence function.

The checking equation of anchorage depth of the anti-sliding device is shown in Eq. (22).

$$\left[\sigma_H\right] = K_H \eta \sigma_C \tag{22}$$

In Eq. (22), K_H is the occurrence coefficient of rock and soil, and η is the reduction coefficient of weathering. Their values in this study are 0.5 and 0.2, respectively.

3. Analysis of the results of the prevention and control plan in the study area

3.1. Analysis of the calculation results of stability

In the study of landslide prevention and control in the natural environment, the stability coefficients calculated by the transfer coefficient method and the strength reduction method are as follows. The stability coefficient obtained by the transfer coefficient method is 1.085, and it is calculated by FESRM is 1.080. The difference rate is 0.5%, which shows that the feasibility of the model is high. The results meet the requirements of the model established in this study.

3.2. Analysis of optimization results of the control plan of landslides

After the front half of the slope is lowered, the checking calculation is carried out. The checking results are as follows: the stability coefficient F_S = 1.021, the stability increased by 2.8% than F_S = 1.003, and this proves that the lowering plan for the first part of the landslide is feasible.

Based on the above calculation model and specific parameters, the residual thrust is a horizontal component, as shown in Fig. 4.

Fig. 4 shows that when the horizontal component of the residual thrust is 1,360 kN/m, the active earth pressure is 887 kN/m. Because the horizontal component of the residual thrust is greater than the active earth pressure, the thrust of the anti-sliding device is taken the residual thrust of 1,360 kN/m. The residual thrust curve of design conditions is located above that of the check working condition, so the design is safe and reasonable.

The calculation results of the internal force of the anti-skid device are shown in Fig. 5.

Fig. 5 shows that the internal forces of the anti-sliding device are the maximum bending moment of 20,123.24 kN m and the maximum shear force of 4,881.01 kN, and the maximum lateral stress is −718.44 kPa.

The calculation result of anchorage depth is that the lateral stress $[\sigma_c]$ = 859 kPa > 718.44 kPa calculated by Eq. (22), so the depth calculation is qualified.

For the rear half of the slope, Midas GTS software is used for checking, and the results are shown in Fig. 6.

Fig. 6 shows that rock and soil in the section have a sign of sliding, and the cracks in the slope are deep. The maximum plastic stress appears at the top of the anti-sliding device, and it has a sign of increasing. The stability coefficient of the cross-section is 1.15 after the sliding is controlled by the anti-sliding device, which is improved to a certain extent, but less than the theoretical value of 1.20. Therefore, it does not meet the requirements and needs to be optimized.

In Fig. 6, the load in the middle and upper parts of the landslide is becoming more and more serious. Therefore, it is necessary to take measures to reduce the load here. The optional methods include adding constraints on the upper part of the anti-sliding device and increasing constraints on the middle part of the slope. The method of adding anchor cables on the anti-sliding device is selected to prevent

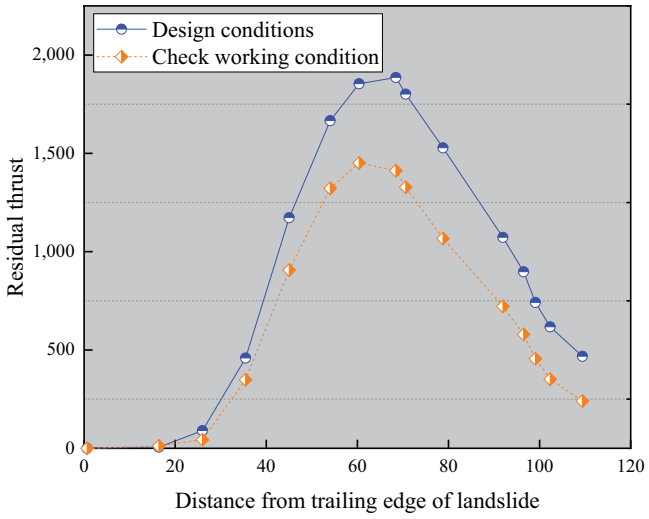

Fig. 4. Residual thrust curve of the section in the middle.

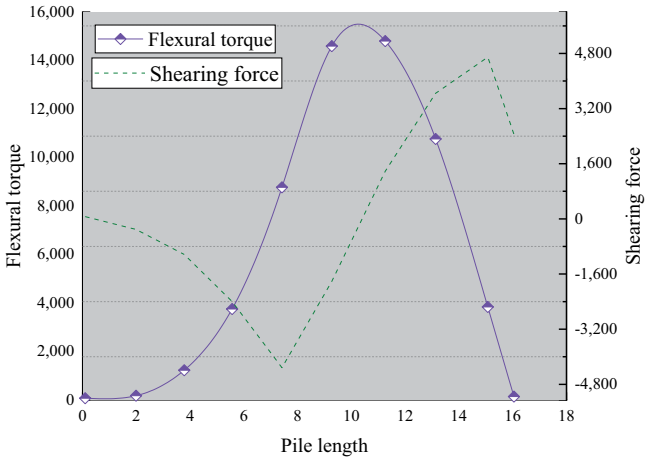

Fig. 5. Calculation results of the bending moment and the shear force of the anti-skid device.

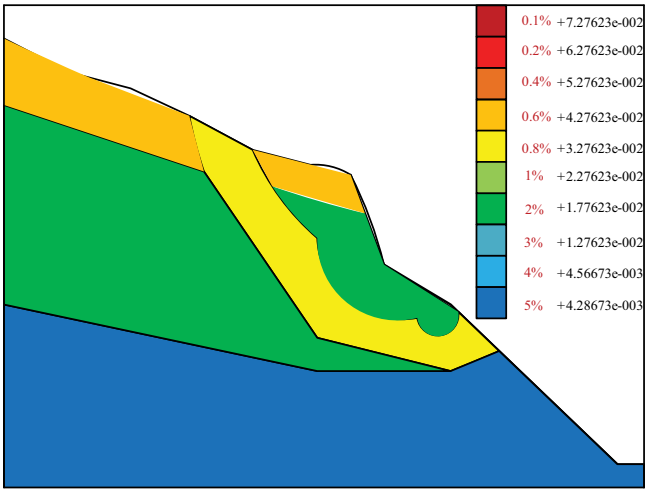

Fig. 6. Equivalent plastic stress program of the anti-skid device after the landslide is controlled.

sliding. The position of the anchor cable is started from the first anti-slide pile of the anti-slide device. The number of an anchor cable is 4, the spacing is 3 m × 3 m, the anchorage length is 9m, the bulk density is 80 kN/m^3, the elastic modulus is 2 × 106 MPa, the Poisson's ratio is 0.25, and the finite element strength reduction Eq. (18) is used for the calculation. The stability coefficient is 1.23 > 1.20, which meets the requirements. Compared with that before the optimization, the stability coefficient increases, which shows that the optimization is feasible and effective.

4. Conclusion

A feasible plan for landslide control is designed in a certain area. The general situation of the study area is analyzed and the relevant parameters of the landslide in the study area are obtained. Qualitative analysis and quantitative analysis are carried out on the stability of the landslide under natural precipitation-free conditions, by the transfer coefficient method and FESRM. On this basis, Midas GTS software is used for modeling, and a two-dimensional model conforming to the landslide in the study area is obtained. To control the landslide in this area, the method of lowering the slope body in the front section of the landslide is used to prevent the sliding, and the anti-skid device is installed at the rear part of the landslide. The results show that the lowered slope body in the front section of the landslide can play a role in anti-skid, and the effect of the anti-skid device at the rear part is not obvious. Therefore, the plan is optimized, that is, the anchor cable is added to the anti-sliding device, and the obvious anti-sliding results are obtained. All the results obtained in this study are qualified. However, the conditions in the study area are not considered comprehensively, and the impact of rainstorms and earthquakes is not analyzed. In the follow-up study, all conditions should be considered as far as possible, so that the research results are universal.

References

[1] M. Van Dyke, T. Klemetti, J. Wickline, Geologic data collection and assessment techniques in coal mining for ground control, Int. J. Min. Sci. Technol., 30 (2020) 131–139.
[2] L. Zou, W. Gui, Simulation and prediction of geologic hazards and the impacts on homestay buildings in scenery spots through BIM, PLoS One, 15 (2020) 0238864, doi: 10.1371/journal.pone.0238864.
[3] B. Choubin, A. Mosavi, E.H. Alamdarloo, F. Sajedi Hosseini, S. Shamshirband, K. Dashtekian, P. Ghamisih, Earth fissure hazard prediction using machine learning models, Environ. Res., 179 (2019) 108770, doi: 10.1016/j.envres.2019.108770.
[4] A. Abdelkarim, A.F.D. Gaber, A.M. Youssef, B. Pradhan, Flood hazard assessment of the urban area of Tabuk City, Kingdom of Saudi Arabia by integrating spatial-based hydrologic and hydrodynamic modeling, Sensors (Basel), 19 (2019) 1024, doi: 10.3390/s19051024.
[5] M.J. Rodríguez-Peces, J.C. Román-Herrera, J. Delgado, M. Tsige, S. Martino, J. Garrido, Unbiased logic-tree data for earthquake-induced landslide hazard maps for low-to-moderate magnitude events, Data Brief, 31 (2020) 105940, doi: 10.1016/j.dib.2020.105940.
[6] S.Y. Bunting, D.J. Lapworth, E.J. Crane, J. Grima-Olmedo, A. Koroša, A. Kuczyńska, N. Mali, L. Rosenqvist, M.E. van Vliet, A. Togola, B. Lopez, Emerging organic compounds in European groundwater, Environ. Pollut., 269 (2021) 115945, doi: doi: 10.1016/j.envpol.2020.115945.
[7] Z. Qing-zhao, P. Qing, C. Ying, L. Ze-jun, S. Zhen-ming, Z. Yuan-yuan, Characteristics of landslide-debris flow accumulation in mountainous areas, Heliyon, 5 (2019) 02463, doi: 10.1016/j.heliyon.2019.e02463.
[8] R. Bipin, B. Prakash, C. Madhukar, C. Sandesh, K. Sushank, K. Saugat, B.P. Padam, Drought stress impacts on wheat and its resistance mechanisms, J. Sustainable Agric., 5 (2021) 67–76.
[9] M. Sakthivadivel, A. Nirmala, J. Sakthivadivel, R.R. Mukhilan, S. Tennyson, Physicochemical and biological parameters of water at industrial sites of Metropolitan City of Chennai, Tamil Nadu, India, Water Conserv. Manage., 4 (2020) 86–94.
[10] I. Sufiyan, K.D. Mohammed, J.I. Magaji, Assessment of crop yield and rainfall simulation in Nasarawa Town Nasarawa State Nigeria, J. Clean WAS, 4 (2020) 75–78.
[11] F. Sun, Y.-P. Zhao, Geomaterials evaluation: a new application of Ashby Plots, Materials (Basel), 13 (2020) 2517, doi: 10.3390/ma13112517.
[12] Y. Ge, H. Tang, X. Gong, B. Zhao, Y. Lu, Y. Chen, Z. Lin, H. Chen, Y. Qiu, Deformation monitoring of earth fissure hazards using terrestrial laser scanning, Sensors (Basel), 19 (2019) 1463, doi: 10.3390/s19061463.
[13] B. Mazzorana, L. Picco, R. Rainato, A. Iroumé, V. Ruiz-Villanueva, C. Rojas, G. Valdebenito, P. Iribarren-Anacona,

D. Melnick, Cascading processes in a changing environment: disturbances on fluvial ecosystems in Chile and implications for hazard and risk management, Sci. Total Environ., 655 (2019) 1089–1103.
[14] J. Wang, S. Zhu, X. Luo, G. Chen, Z. Xu, X. Liu, Y. Li, Refined micro-scale geological disaster susceptibility evaluation based on UAV tilt photography data and weighted certainty factor method in Qingchuan County, Ecotoxicol. Environ. Saf., 189 (2020) 110005, doi: doi: 10.1016/j.ecoenv.2019.110005.
[15] B. Liu, S. Han, H. Gong, Z. Zhou, D. Zhang, Disaster resilience assessment based on the spatial and temporal aggregation effects of earthquake-induced hazards, Environ. Sci. Pollut. Res. Int., 27 (2020) 29055–29067.
[16] L. Han, Q. Ma, F. Zhang, Y. Zhang, J. Zhang, Y. Bao, J. Zhao, Risk assessment of an earthquake-collapse-landslide disaster chain by Bayesian Network and Newmark Models, Int. J. Environ. Res. Public Health, 16 (2019) 3330, doi: 10.3390/ijerph16183330.
[17] E.Y.Y. Chan, A.Y.T. Man, H.C.Y. Lam, Scientific evidence on natural disasters and health emergency and disaster risk management in Asian rural-based area, Br. Med. Bull., 129 (2019) 91–105.
[18] C.B. Eng, W.L. Tan, Disaster prevention and recovery, Methods Mol. Biol., 1897 (2019) 31–41.